The ISOCAM Parallel Mode*

Ralf Siebenmorgen[1], Norbert Schartel[2], and Stephan Ott[1]

[1] ESA/ISO Data Centre, Villafranca del Castillo, P.O. Box 50727, E-28080 Madrid
[2] ESA/ XMM Operation Centre, Villafranca del Castillo, P.O. Box 50727, E-28080 Madrid

Abstract. The mid infrared camera (ISOCAM) on board of the infrared space observatory (ISO) routinely exposed the sky during non prime observations. This so called ISOCAM parallel mode gives the largest data set of ISO. It represents more than 40% of all ISO observations. We present the calibration strategy of the ISOCAM parallel mode and discuss statistical properties of the extracted sources. Having analysed about 40% of the data we demonstrate that our point source catalogue should contain more than $\sim$ 50.000 sources at a limiting flux down to $\sim$ 3mJy, all found at a confidence level well above 95%. From the source catalogue we identified the asteroid Watsonia.

1 Introduction

During all pointed observations of ISO (Kessler et al., 1986) when the infrared camera ISOCAM (Cesarsky et al., 1996) was not the prime instrument it still routinely exposed to the sky. In the so called parallel mode, ISOCAM pointed, depending on the prime instrument, between 10' and 20' away from the prime target. Thus enabling to perform an effectively unbiased survey of limited areas of the infrared sky at high sensitivity (Siebenmorgen et al., 1996). Up today there are 42604 ISOCAM parallel mode observations in the ISO archive so that this survey amounts to about 40% of all observations performed during the ISO life time. In the parallel mode, ISOCAM was configured using the 6.7 μm broad band filter lw2 or 6.0 μm narrow band filter lw4, both at 6" pixel resolution giving a 180"$\times$180" total field of view. In addition during calibration revolutions the 14.3 μm broad band filter lw3 at 1.5" pixel scale was applied, which led to a 48"$\times$48" field of view. The spatial resolution of ISOCAM thus converts to about a 15 fold increase of angular resolution as compared to IRAS.

Compared to the ISO prime instrument, not the full telemetry rate of the satellite was available during parallel mode observations and a number of 12$\times$2.1s exposures have been co-added on-board so that every 25.2s a single exposure was down-linked to the ground segment. During one observation on a single sky position the typical (median) integration time is about 6 minutes.

* Based on observations with ISO, an ESA project with instruments funded by ESA Member States (especially the PI countries: France, Germany, the Netherlands and the United Kingdom) with the participation of ISAS and NASA.

In this article we present statistical properties of a first generation catalogue of point sources detected by ISOCAM in its parallel mode. The data analysed until now are 300 ISO revolutions, this represents about 40% of the total data available. During those 300 revolutions filters lw3 and lw4 have been configured about 13% each but filter lw2 was more frequently applied (74%). Therefore we restrict our statistical discussion here to lw2 observations.

2 Data processing

We start calibration of the images from SPD level in the CIA [1] environment and apply basic calibration steps, consisting of dark correction, deglitching, co-addition of exposures on the same sky position, flat fielding and photometry conversion. (Principles on ISOCAM data are described by Siebenmorgen et al., 1999). However before calibration of images care has to be taken in the precision of the software which relates the ISO satellite time key to the ISOCAM instrument time key. Here we have been using an updated version of the standard off line processing system (OLP8). In addition already on raw data (ERD) level we check for saturated detector pixels. Those pixels have been flagged and are not considered for reliable source extraction still 10 minutes after pointing away from the saturation source. During observations a saturation avoidance procedure has been applied by the ISO operators so that only a small number of detector saturations occurred.

The most reliable deglitching is done by studying the time history of the signal of a single pixel. This limits us to analyse only data sets having more than 3 individual exposures. For cosmic ray suppression we applied an adaptive sigma-clipping method (Ott et al., this volume) . The accuracy of the flat fields limits the faint source extraction. To improve the quality more than 100 different sky flats derived from suitable ISOCAM prime observations have been re-calibrated. This allows to group the flats of a single optical configuration into a number of different flat field families (Ott et al., this volume). Caused by the lens wheel jitter the most dramatic changes of the flats occurred at the outer parts on the array. Consequently we chose for each image the flat field which minimises the RMS at the boarder of the detector.

3 Extraction of source candidates

From the calibrated images we extract source candidates by considering the point spread function and the RMS image. We applied the multi wavelet

[1] CIA is a joint development by the ESA Astrophysics Division and the ISOCAM Consortium led by the ISOCAM PI, C. Cesarsky, Direction des Sciences de la Matiere, C.E.A., France. Contributing ISOCAM Consortium institutes are Service d' Astrophysique (SAp, Saclay, France) and Institute d' Astophysique Spatiale (IAS, Orsay, France)

transform algorithm by Starck et al. (1998) and retrieve all source candidates for which the standard deviation of the noise is more than 4 σ and where the 1σ uncertainty of the location of the object on the array is smaller than 3 pixels. As second step we check the temporal signal behavior for each source candidate. For this we estimate the flux error for each exposure (σ_i), by assuming that the flux F_i to the next good flux estimate F_{i+1} is within $\sim 1\sigma_i$. All candidates where

$$2.5 \cdot (\sum_{i=1}^{N} \sigma_i^2)^{\frac{1}{2}} \leq \sum_{i=1}^{N} F_i - N \cdot B \tag{1}$$

are considered to be spurious and therefore rejected. Here $\sigma = \sqrt{\sum_{i=1}^{N} \sigma_i^2}$ and the background B is estimated by applying a 7×7 pixel median box filter over the image. As third step we apply a statistical analysis over all remaining source candidates, which is subject of the following Section.

4 Statistical properties of the source catalogue

For each source candidate, retrieved with the procedure discussed in the previous section, we calculate a confidence level. The goal is to define *cut–of–parameters*, such as a limiting flux, which allows to extract sources at a confidence level above 95%.

As a first step we consider all sources observed in at least two pointings. This means we consider a source candidate S in pointing P_1 and select all pointings P_2 where candidate S should be re-observed. In P_2 we measure the distance D from the nominal position of S to all source candidates retrieved from image P_2. This we do for all our source candidates and plot the histogram of all those distances D. Such a plot we call from here on *coincidence histogram.* We expect three cases:

- If $D \leq 1$ pixel, the source candidate S was likely to be re-observed in P_2.
- If 1 pixel $\leq D \leq$ 2–3 pixels, the source candidate S was most likely re-observed, however caused by the lens wheel jitter the absolute astrometry of S is shifted relative to P_1.
- If $D > 3$ pixels, we measure the background.

The background at this point is of complicated structure, it contains:

1. True background sources, such as stars.
2. Spurious detections, such as residual cosmic ray hits of the detector not masked by our temporal deglitching method.
3. Variable targets, such as asteroids.

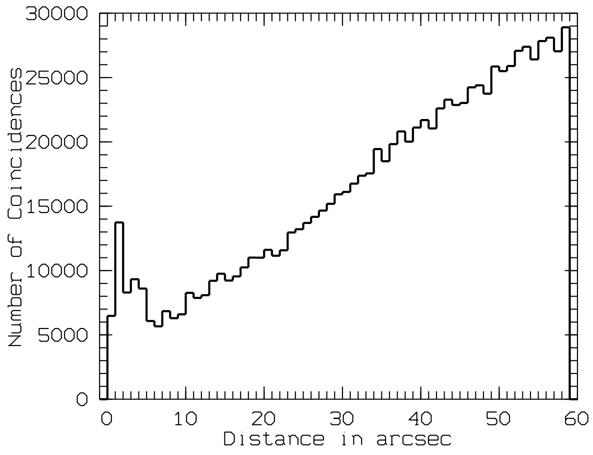

Fig. 1. Coincidence histogram of all source candidates as retrieved by the procedure discussed in Section 3. The confidence of sources found at a distance $D \leq 6$" is not much above 50%.

We expect to see in the coincidence histogram a peak close to $D \sim 0''$, a secondary peak at $D \sim 12''$ and overlaid a linear function which represents the background. The integral of the first peak divided by the integral of the interpolated background under this peak gives the *confidence* level. In Fig. 1 we show the coincidence histogram of the input catalogue (as retrieved from Section 3). One notice a strong linear background over a small peak centered around $D \sim 2''$. The confidence level is just above 50%. This indicates that still after a careful calibration effort of the images the so far retrieved source candidates have a high probability to be spurious. At this point one could for example identify some of the source candidates by cross correlation with other catalogues, e.g. DENIS, and extract at least some real sources. However, our aim is to provide a catalogue with a confidence level for each source sufficient for further scientific analysis. For example from the wavelet analysis one can relate the inter-crossing coefficients of the different wavelet scales to the physical size of the source (Starck et al. 1999). The histogram of this parameter, which we call for simplicity "glitch", is shown in Fig. 2a. It shows a quite smooth distribution but a singularity at glitch ~ 0. Looking at the coincidence histogram (Fig.2b) of source candidates having in at least one pointing glitch ~ 0, proves that they are within all statistical limits spurious.

As second example we investigate the histogram of the retrieved source fluxes (Fig.3a). We find a sharp cut-off at a flux of $\sim$ 1mJy. We plot in Fig. 3b

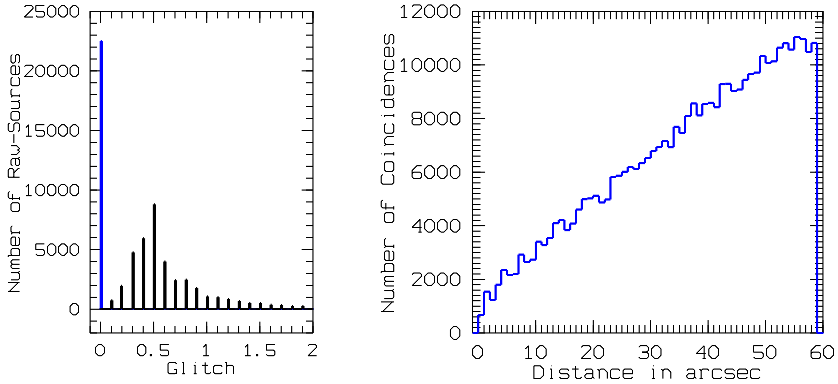

Fig. 2. a) Histogram of the inter-crossing wavelet coefficient which we call "glitch". This function is smooth but shows a singularity at glitch close to zero. (left). b) Coincidence histogram of all sources with glitch ~ 0. Within the statistical limit all those sources can be regarded as spurious.

the coincidence histogram of all source candidates which are found below the expected limiting flux ($\geq$ 1.5 mJy) of ISOCAM starring observations (The ISOCAM Team, 1996) in at least one pointing. Again one notice that all those sources are spurious.

At this point the background in the coincidence histograms is significantly reduced. It becomes difficult to distinguish real and spurious components of the measured background. We therefore look back to the detector geometrie to find an area and a procedure allowing to suppress the background: Considering the lens wheel jitter, which is ~ 2 pixels, we need to neglect in our analysis the boarder of the detector. Caused by the dead column (which is column 23) we should consider only the detector area up to column (23-2). From the center of the detector (column 15) we are left with a radius of $23 - 2 - 15 = 7$ pixels (42"), which is never influenced by detection problems caused by the boarder or the dead column; also still by considering the lens wheel jitter. We then calculate the coincidence histograms, but with a slightly modified procedure:

1. We select a source S in pointing P_1 which is detected between columns $9 - 15$ and rows $9 - 25$. This is the detector area surely free of boarder problems.

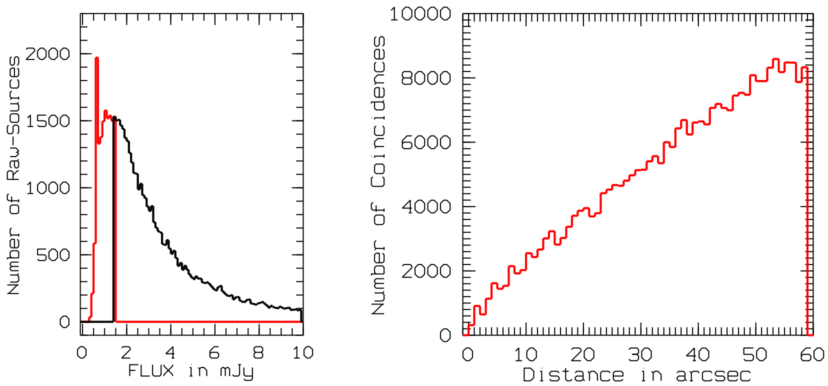

Fig. 3. a) Histogram of the source fluxes. For starring observation the limiting flux is above 1.5 mJy (left). b) Coincidence histogram of all sources with fluxes less than the predicted sensitivity limit. Within the statistical limit all those sources can be regarded as spurious.

2. We consider only those sources S in P_1 where no further source is detected in a circle with radius of 7 pixels. This should suppress most of the background.
3. We select all pointings P_2 where source S should be re-observed at a nominal position on the detector as defined in 1.
4. In P_2 we measure the distance D from the nominal source position of S to all other source candidates. However since we need to consider once more the lens wheel jitter we measure source distances in P_2 only up to a radius of 5 pixels from the nominal source position of S.

The coincidence histogram should give a peak at $D \leq 1$ pixel (6") of at most real sources and a secondary peak at $\sim$ 2 pixels. The secondary peak is caused by the lens wheel jitter. The coincidences for $D > 20''$ should be almost free of true background sources except a few. The few remaining real background sources are those which are not detected in P_1 because of different sensitivity limits, e.g. integration times in both images; - suppose the case that only a minimum number of exposures are taken in P_1 but a much larger integration time was spend on P_2. The definition of the confidence level of the sources remains the same as given above. After fine tuning the cut of parameters we show in Fig. 4 the coincidence histogram. We show this only

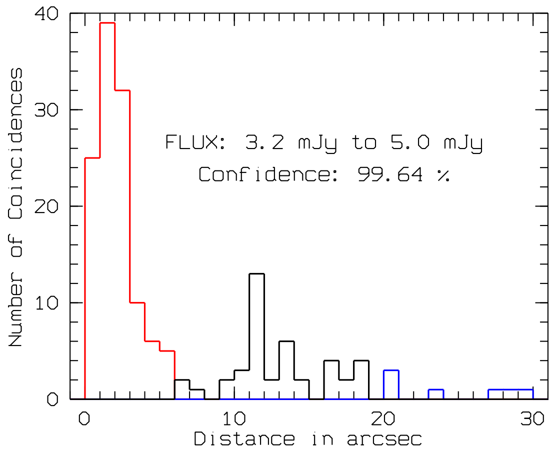

Fig. 4. Coincidence histogram of sources close to the predicted sensitivity limit of starring observations. We applied a method to suppress the background and fine tuned the cut of parameters from the input list of source candidates (see text). The interpolation of sources detected between 20" – 30" to distances $D \leq 6''$ represents the number of spurious detections. We proof that our remaining source candidates have a confidence above 95%.

for sources close to the theoretical detection limit (3.2 – 5 mJy) and still calculate a confidence level of the sources around 99.6%.

We so far have used only a pure statistical analysis so that we can apply the retrieved cut of parameters to the full input catalogue of source candidates. If we further extrapolate the number of the remaining sources to the full data base of ISOCAM parallel mode observations we expect a total of $\sim$ 50.000 sources extracted from lw2 observations at a confidence limit well above 95% and at a limiting flux close to the predicted sensitivity limit.

5 Time variable sources: Asteroid Watsonia

We are left to discuss time variable source as a contribution to the background structure measured in the coincidence histograms. Together with T.G. Müller, we detected in the parallel mode image observed on the 13 Feb 1998 at 18:20:00 UTC two sources (Fig. 5). One of the source can be identified by a star and the other is a time variable source which coincides with the predicted orbital position of the asteroid *Watsonia*. From the orbital elements (Müller & Lagerros, 1998) a flux of $F_{pre} = 100 \pm 10$mJy is predicted. Considering a

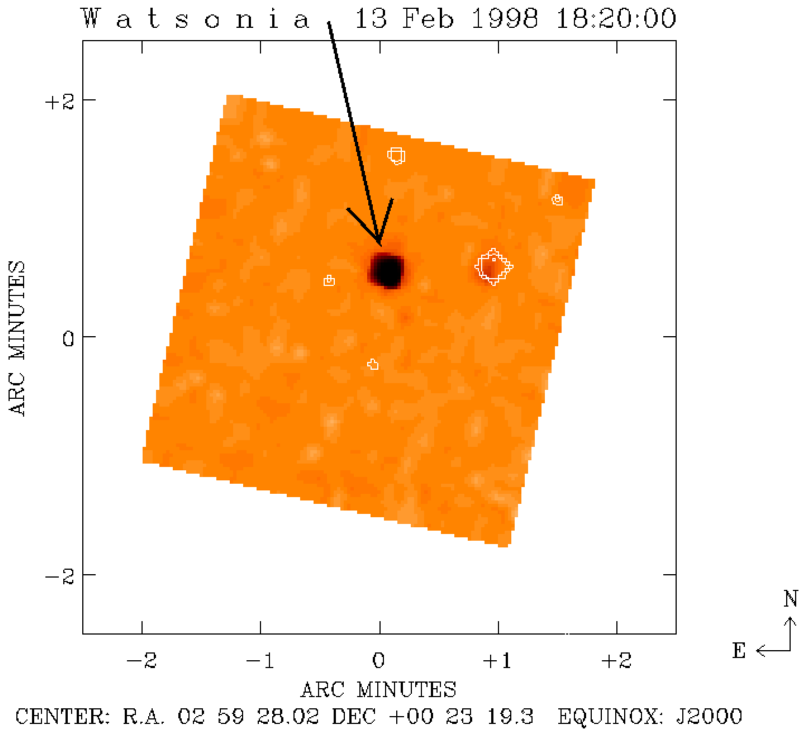

Fig. 5. ISOCAM image observed at 13 Feb 1998, 18:20:00 UTC. Contours represent an overlay of the digitized sky survey. We detect asteroid Watsonia at a flux of ~ 150mJy.

colour correction factor of 1.15 we measure in our ISOCAM data a flux of 115 ± 15mJy.

References

1. Cesarsky C., Abergel A., Agnèse P. et al., 1996, A&A 315, L32
2. Kessler M.F., Steinz J.A., Anderegg M.E. et al., 1996, A&A 315, L27
3. Ott S., Pollock A., Siebenmorgen R., *this volume*
4. Müller T.G., Lagerros J., 1998, A&A 340, 338
5. Siebenmorgen R., Abergel A., Altieri B., et al., 1996, A&A 315, L169
6. Siebenmorgen R., Blommaert J., Sauvage M., Starck J.-L., 1999, ISO Handbook Volume III (CAM), SAI – 99 – 057/Dc, http://www.iso.vilspa.esa.es/
7. Starck J.L., Murtagh F., Bijaoui A., Image Processing and Data Analysis: The Multiscale Approach, Cambridge University Press, Cambridge (GB), 1998, (http://www.multiresolution.com)
8. The ISOCAM Team, 1996, "ISOCAM Observer's Manual", ESA/ESTEC